Enhancement of Surface Properties of 316L Stainless Steel with Silver Nanoparticles using Airbrush Spray Process

Gizem KARABULUT[1*], Nuray BEKÖZ ÜLLEN[1], Selcan KARAKUŞ[2]

[1] Istanbul University-Cerrahpaşa, Faculty of Engineering, Department of Metallurgical and Materials Engineering, İstanbul, Turkey.
[2] Istanbul University-Cerrahpaşa, Faculty of Engineering, Department of Chemistry, İstanbul, Turkey.

Abstract

In this study, the surfaces of 316L stainless steel, which is frequently preferred in biomedical applications, were modified with silver nanoparticles (Ag NPs) to improve their antibacterial and anticorrosive properties. Firstly, Ag NPs were synthesized using a completely green a plant-mediated ultrasound-assisted synthesis method and characterized. Next, Ag NPs were coated onto the surface of the 316L with the airbrush spray technique. The coated surfaces were examined by SEM, surface roughness, profilometer, optical microscope, electrochemical corrosion, and disk diffusion analyses. The average surface roughness values of the surface modified samples were found to be moderately suitable for use in biomaterials while exhibiting corrosion resistance and antibacterial resistance. The Ag NPs coating offers significant potential for biomedical applications.

Keywords: multifunctional coating, antibacterial, biometal, nanotechnology.

Püskürtme Kaplama Tekniği ile 316L Paslanmaz Çeliğin Yüzey Özelliklerinin Gümüş Nanopartiküllerle İyileştirilmesi

Öz

Bu çalışmada, biyomedikal uygulamalarda sıklıkla tercih edilen 316L paslanmaz çelik yüzeyinin antibakteriyel ve antikorozif özelliklerini geliştirmek amacıyla yüzeyleri gümüş nanopartiküllerle (Ag NPs) modifiye edildi. İlk olarak gümüş nanopartiküller tamamen çevreci bir yolla bitki aracılığıyla sonikasyon yöntemiyle desteklenerek sentezlendi ve karakterize edildi. Ardından çeliğin yüzeyine püskürtme yöntemiyle kaplandı. Kaplanan yüzeyler SEM, yüzey pürüzlülük, profilometre, optik mikroskop, elektrokimyasal korozyon ve disk difüzyon analizleriyle incelendi. Kaplanmış numunelerin yüzey pürüzlülük değerleri biyomalzemelerde kullanım için orta derece sınıfa uygunluk gösterirken, korozyon dayanımı ve antibakteriyel davranış sergilediği tespit edildi. Gerçekleştirilen kaplama biyomedikal uygulamalar için önemli bir potansiyel sunmaktadır.

Anahtar Kelimeler: multifonksiyonel kaplama, antibakteriyel, biyometal, nanoteknoloji.

*Corresponding Author: gizem.karabulut@iuc.edu.tr
Gizem KARABULUT, https://orcid.org/0000-0003-0930-5380
Nuray BEKÖZ ÜLLEN, https://orcid.org/0000-0003-2705-2559
Selcan KARAKUŞ, https://orcid.org/0000-0002-8368-4609

1. Introduction

Metals and their alloys are generally preferred for biomedical implants that require high strength and load-bearing capacity. Among them, SS316L is the most preferred group. SS316L is preferred over other biometals because of its high toughness and strength. It is also economical, easy to find, and easy to manufacture [1,2]. Therefore, thanks to their high mechanical properties, they offer confidence in load-bearing applications (e.g. screws, pins, plates, hip, knee, and dental prostheses) [3]. However, SS316L behaves bioinert to body tissues, is very susceptible to corrosion by body fluids, and bacteria can easily attach to its surface and form biofilms [4,5]. To reduce or eliminate these problems, surface coating is an effective, simple, and applicable method [6].

In recent years, metallic nanoparticles (NPs)-based surface coatings have been used to improve the surface properties of SS316L [7]. Metallic NPs have gained importance in surface coatings because of their advanced properties at nanoscale [8]. Among these, silver nanoparticles (Ag NPs) are at the forefront of surface coating applications due to their advanced conductivity, catalysis, chemical, physical, and known superior antipathogenic properties [9,10]. The synthesis methods for surface coatings based on NPs, to be used in biomedical applications, are very important. This is because it's come into direct or indirect contact with living tissue. The synthesis methods for Ag NPs can be mainly divided into physical, chemical, and biological methods [11,12]. Among the biological methods, plant-mediated synthesized Ag NPs are important for use in the biomedical field. In plant-mediated synthesis of Ag NPs, the synthesis process is carried out using the extract of the whole plant or specific parts such as leaves, stems, roots, and seeds. Plant extracts contain secondary metabolites such as phenolic acids, flavonoids, and terpenoids that are selective for metallic ions and enable the formation of NPs. These metabolites are used as reducing agents [13]. The synthesis of Ag NPs from plant sources involves purification of the bioreducing agent and controlled mixing with the precursor metal solution. Then, reactions take place at room temperature leading to the formation of Ag NPs [13,14]. To increase the efficiency of plant-mediated synthesis, supports such as temperature, mixing or ultrasound irradiation can be applied. In recent years, recent studies have been carried out on the synthesis of Ag NPs with ultrasound-assisted plant-mediated synthesis technique [15–17]. This is due to the fact that the method is an economical, fast, easy, and high efficiency method.

The development of advanced coatings for SS316L has become increasingly important in recent years due to its widespread use in various industries, especially in biomedical implants. Multifunctional properties can be achieved by modifying bio-metallic surfaces with NPs using various coating methods such as sol-gel [18], drop casting [7], electrodeposition [19], and chemical vapor deposition [20]. One promising method is the airbrush spray coating method, which offers a simple and cost-effective approach for enhancing the surface properties of biometals. Today, the airbrush spray coating method is a popular method for applying to solar panels or electrodes. There are also pioneering studies on its use for coating metal surfaces [7,21]. The method involves using a nozzle to spray the solution at a specific pressure, resulting in an efficient, easy, fast, and eco-friendly process for biomedical applications [7,22,23]. Based

on the literature, the airbrush spray coating technique was used to investigate the effectiveness of Ag NPs coating on the surface of SS316L for improving its antibacterial and anticorrosive properties. For this purpose, Ag NPs were synthesized using matcha tea extract through the ultrasound-assisted method. The PEGylated matcha tea extract-silver nanoparticles (PEG400/MTE-Ag NPs) were then coated onto the surface of SS316L using the airbrush spray coating technique. The coated surface was evaluated for its morphological features, surface roughness, coating thickness, and distribution, as well as its antibacterial and anticorrosive properties using disc diffusion and electrochemical polarization tests, respectively. The results from this study suggest that the Ag NPs coated SS316L exhibits promising qualitative corrosion and antibacterial behavior that can be useful in medical applications. Therefore, this study aims to address the knowledge gap in the literature and provides detailed information on the synthesis and coating of Ag NPs on SS316L using the airbrush spray technique.

2. Material and Methods

2.1. Materials

The matcha tea powder was purchased from Arifoğlu Company (Turkey) and is known as *Camellia sinensis L.,* the plant commonly used to produce green tea. $AgNO_3$, sodium hydroxide (NaOH) (MW: 40.00 g/mol), and ethanol (EtOH, purity $\geq$%99.4) were supplied from Merck Company (Germany). Polyethylene glycol (PEG) (MW: 400 kDa) was purchased from Fluka Company (Switzerland). SS316L was obtained from Birçelik Company (Turkey) with a diameter of 28 mm and a length of 1 m. The chemical constituent values are taken from the technical inspection certificate of the Birçelik Company and chemical constituent of SS316L is presented in **Table 1**.

Table 1. The chemical constituent of SS316L (wt.%).

C	Ni	Cr	Mo	Si	Mn	Cu	S	P	N	Fe
0,014	10,091	16,581	2,048	0,437	1,317	0,326	0,024	0,025	0,041	Balance

### 2.2. Natural plant-mediated ultrasound-assisted synthesis of Ag NPs

Matcha tea powder was used for the bio-sono synthesis of Ag NPs. The matcha tea powder underwent purification with distilled water before being dried in a vacuum oven (60°C, 2 h). After adding 5 g of the dried sample to 100 g of distilled water, the mixture was stirred (500 rpm, 30 mins). After a homogeneous mixture was obtained, it was kept in a dark environment (3 days, 25 °C). Finally, the extract was obtained by decantation and filtration.

20 mL of the prepared matcha extract (MTE) was taken, 0.1 g of PEG was added and mixed (10 min, 500 rpm). $AgNO_3$ (0.1 g) was dissolved in 50 mL of distilled water, then stirred (10 min, 25 °C). After dissolving of NaOH (0.2 g) in 50 mL of distilled water, the sample was stirred (10 min, 25 °C). The process involved adding 4 mL of NaOH solution and 50 mL of $AgNO_3$ solution dropwise into the PEG400/MTE solution, followed by mixing (10 min, 25 °C, and 500 rpm). The resulting mixture was then subjected to sonication (30 mins, 50% amplitude)

using a Sonopuls HD3100 Bandelin device. The PEG400/MTE-Ag NPs solution was then filtered using a sterile 0.22 µm filter to complete the process.

2.3. Airbrush spray coating of the SS316L

Before the coating process, SS316L in bar form was sliced to obtain disk form by computer numerical control machine (CNC). The SS316L substrate (thickness: 2 mm, diameter: 25 mm) was cleaned in an ultrasonic bath and then dried in an oven (10 min, 60 °C). Piston type airbrush compressor kit (Model: AS186) was used in the coating process. The spray gun's nozzle tip is 0.2 mm. During the spraying process, a 28 mm diameter plastic pipe was used to prevent the solution from splashing around and to provide spraying from an equal distance to the surface. The prepared coating solutions were filled into the chamber and then sprayed on all substrate surfaces with an auxiliary device from a distance of 75 mm at 3 bar and for 4 secs. **Fig. 1** provides an overview of the experimental steps used to coat the SS316L with PEG400/MTE-Ag NPs.
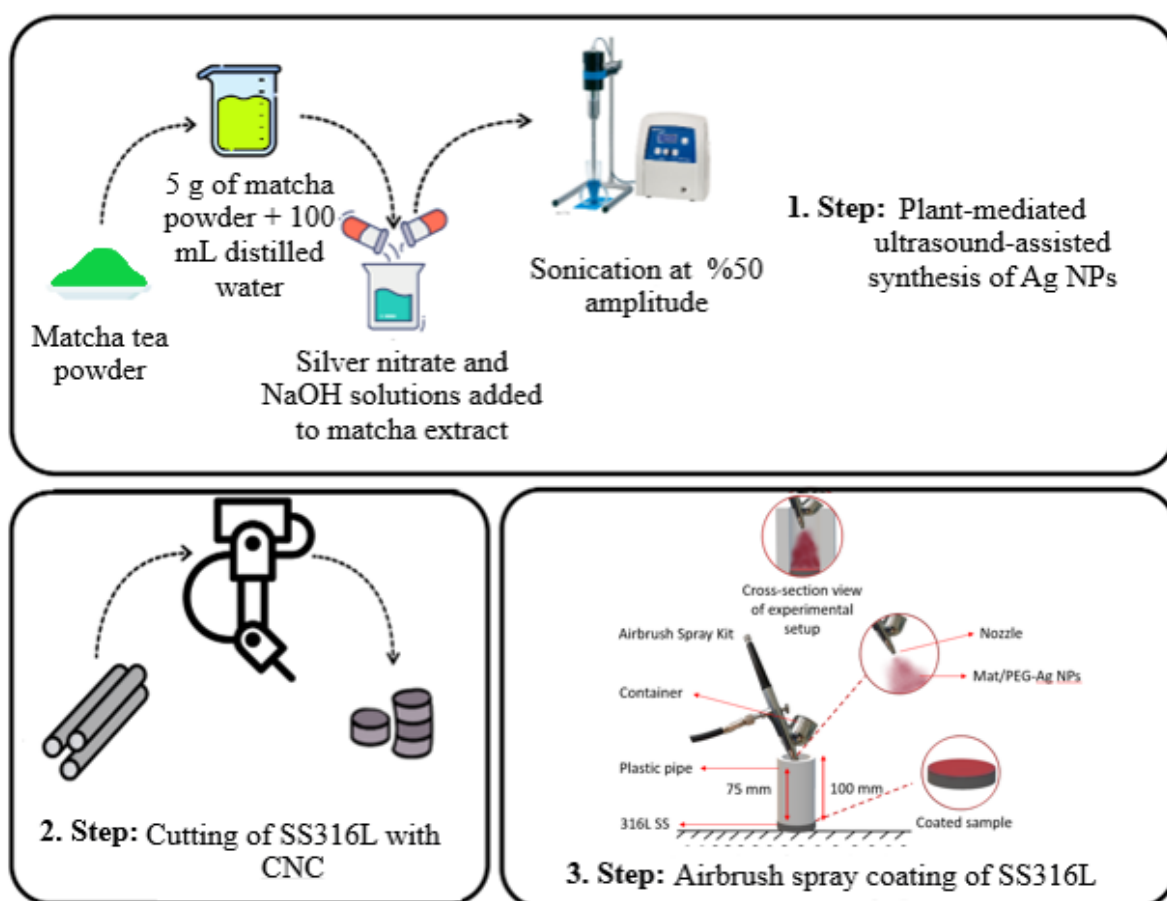
Figure 1. Schematic diagram of the process stages of the preparation of PEG400/MTE-Ag NPs coated SS316L

2.4. Characterizations

In this study, the first MTE-based synthesis of Ag NPs was performed and characterized to obtain chemical, physical, and morphological properties of the PEG400/MTE-Ag NPs. Ultraviolet-visible spectrophotometry (UV-Vis), X-ray diffraction (XRD), X-ray

photospectrometer (XPS), and transmission electron microscopy (TEM) techniques were used to characterize the synthesized NPs. Optical properties investigations of the Ag NPs were performed with a dual-beam UV-Vis spectrophotometer (PG Instruments, T + 80 model) using UVWin 5 software. Crystal structure of the NPs were performed with Rigaku D/Max2200/PC XRD device (Cu-Kα beam operated at 40 kV, 15 mA, between 0° and 70°). The chemical properties and valence electron states of the PEG400/MTE-Ag NPs were determined using a Specs-Flex device for XPS analysis (Al-Kα radiation). The morphological characterization of synthesized PEG400/MTE-Ag NPs was investigated TEM (Hitachi High Tech HT7700 device). The crystalline size of the Ag NPs was calculated using the Eq.2.1.

$$D_p = \frac{0.94.\lambda}{\beta.\cos\theta} \tag{2.1}$$

The Eq. 2.1 includes the following variables: X-ray wavelength (λ: 0.154), full width half maximum (FWHM) (β), crystallite size diameter (D), and Bragg diffraction angle (2 Theta).

Various methods were used to characterize the surfaces of SS316L substrates coated with PEG400/MTE-Ag NPs using an airbrush spray coating process. The distribution, morphology, and sizes of PEG400/MTE-Ag NPs on the SS316L surface were investigated by SEM (Zeiss-Sigma 300 device). The thickness of coating and distribution of coating on the sample surface were examined using an optical microscope (Nikon Eclipse MA100). For the measurement of changing of surface roughness after coating, surface roughness measurements of coated and uncoated surfaces were carried out using Mitutoyo Surftest SJ-210 device. The profilometer (Kla Tencor Stylus Profiler P7 Model) was used to examine the 3D particle distribution and thickness measurements of NPs coated SS316L surfaces.

2.4.1. Antibacterial assay

The agar well diffusion technique was indeed used to investigate the antimicrobial effect of the uncoated and Ag NPs coated on SS316L samples against *Escherichia coli* (*E. coli*) and *Staphylococcus aureus* (*S. aureus*) bacterial strains. Details on the preparation of bacterial cultures were given in our previous study [7]. 75 µL of the prepared cultures were spread on Tryptic soy broth (TSB)-agar plates, then the samples were placed. After incubation (16 h, 37°C), the size of the zone of inhibition (ZOI) was measured using a ruler.

2.4.2. Electrochemical corrosion performance

The anticorrosive performance of the PEG400/MTE-Ag NPs coating on the SS316L was investigated using a Gamry brand Interface 1000 model computer-aided potentiostat. Electrochemical corrosion analysis was performed using Ringer's solution in a 1000 mL cell using a conventional three-electrode system (working electrode: samples, counter electrode: high density graphite, and reference electrode: saturated calomel electrode). Ringer's solution (pH=5.9) was prepared with two Ringer tablets (Merck Company) and a magnetic stirrer in 1000 mL of distilled water. Each Ringer's tablet consists of 2.25 g/L NaCl, 0.105 g/L KCl, 0.06 g/L anhydrous $CaCl_2$, and 0.05 g/L $NaHCO_3$. Software such as Framework and Echem Analyst Gamry were employed for research methodology. In our previous studies [7], the study was further explained. By polarizing all samples between -250 mV and +250 mV at a scan rate of 1.0 mV/min, Tafel performed measurements.

3. Results and Discussion

3.1. Characterization results of the synthesized PEG400/MTE-Ag NPs

The UV-Vis analysis was used to investigate the absorbance measurements and particle distribution of Ag NPs, while the XRD analysis was used to examine the crystal structure and particle size of Ag NPs in the nanostructure of nanostructure synthesized through plant-mediated sonochemical method. UV-Vis and XRD spectra are given in **Fig. 2a** and **b**. PEG400/MTE-Ag NPs exhibited a broad peak between 331 nm and 502 nm with a peak at 420 nm in UV-Vis spectrum (**Fig. 2a**). This absorbance band due to formed by surface plasmon resonance (SPR) is typical for Ag NPs [7,24,25]. The width of the spectrum is an indication that the Ag NPs exhibit a polydisperse distribution. In the XRD graph of Ag NPs (**Fig. 2b**), it was observed that peaks occurred at 24.02°, 38.18°, 44.32°, and 64.52°. It corresponds to the (111), (200), and (220) planes of silver. These planes show that the silver in the structure is in the FCC structure. The peak formed at 24.02° caused by the organic phases in the PEG400/MTE-Ag NPs in the Ag NPs structure [26–28]. Using the **Eq. 2.1**, the size of the crystallite size of Ag NPs was calculated to be 27.45 nm.
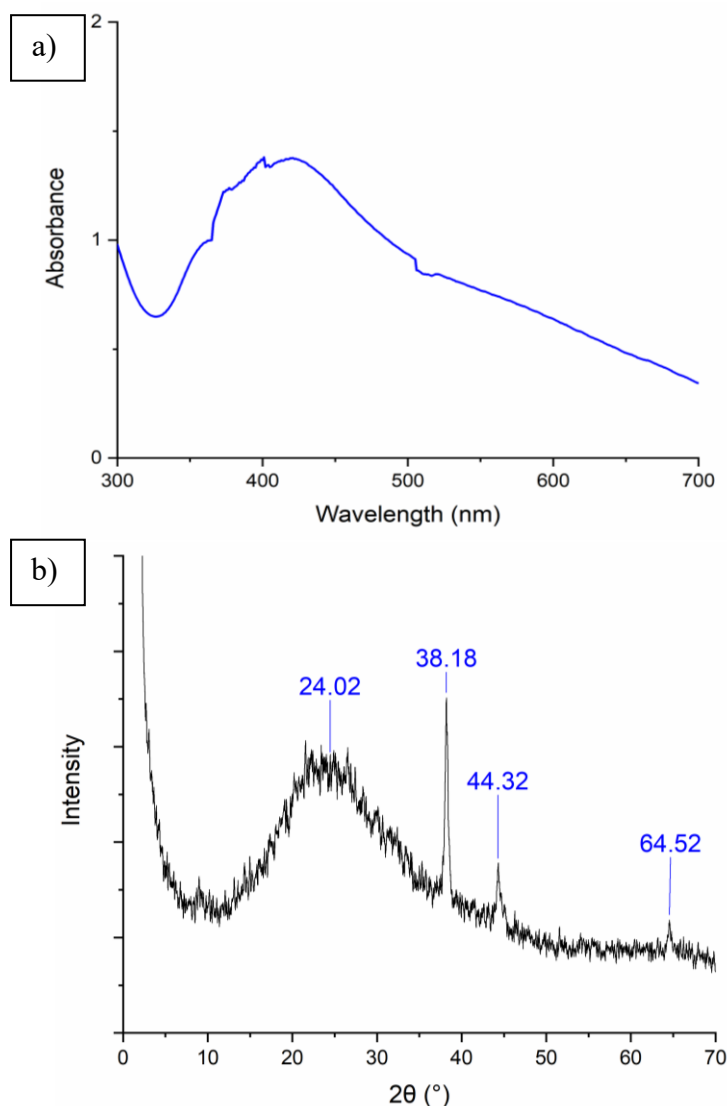
**Figure 2.** a) UV-Vis and b) XRD graphs of the PEG400/MTE-Ag NPs

The analysis of the valence electrons and oxidation states of elements in the nanostructure was carried out using XPS. In **Fig. 2**, XPS graphs of Ag NPs for (a) general, (b) oxygen, (c) carbon, and (d) silver elements are given. The O1s spectrum (**Fig. 2b**) showed a distinct peak at 530.40 eV. The C1s spectrum (**Fig. 2c**) showed two peaks at approximately 283.10 eV and 291.50 eV, respectively. The spectrum of Ag3d of the prepared Ag NPs (**Fig. 2d**) was observed as two peaks with values of approximately 372.2 eV and 366.30 eV. These peaks correspond to the 3d/2 and 5d/2 orbitals of metallic silver, respectively. The oxygen and carbon content originated from the organic matrix structure. The Ag peaks show that the silvers in the structure without oxidation are completely in metallic form. XPS results are consistent with the literature [18,25,29].
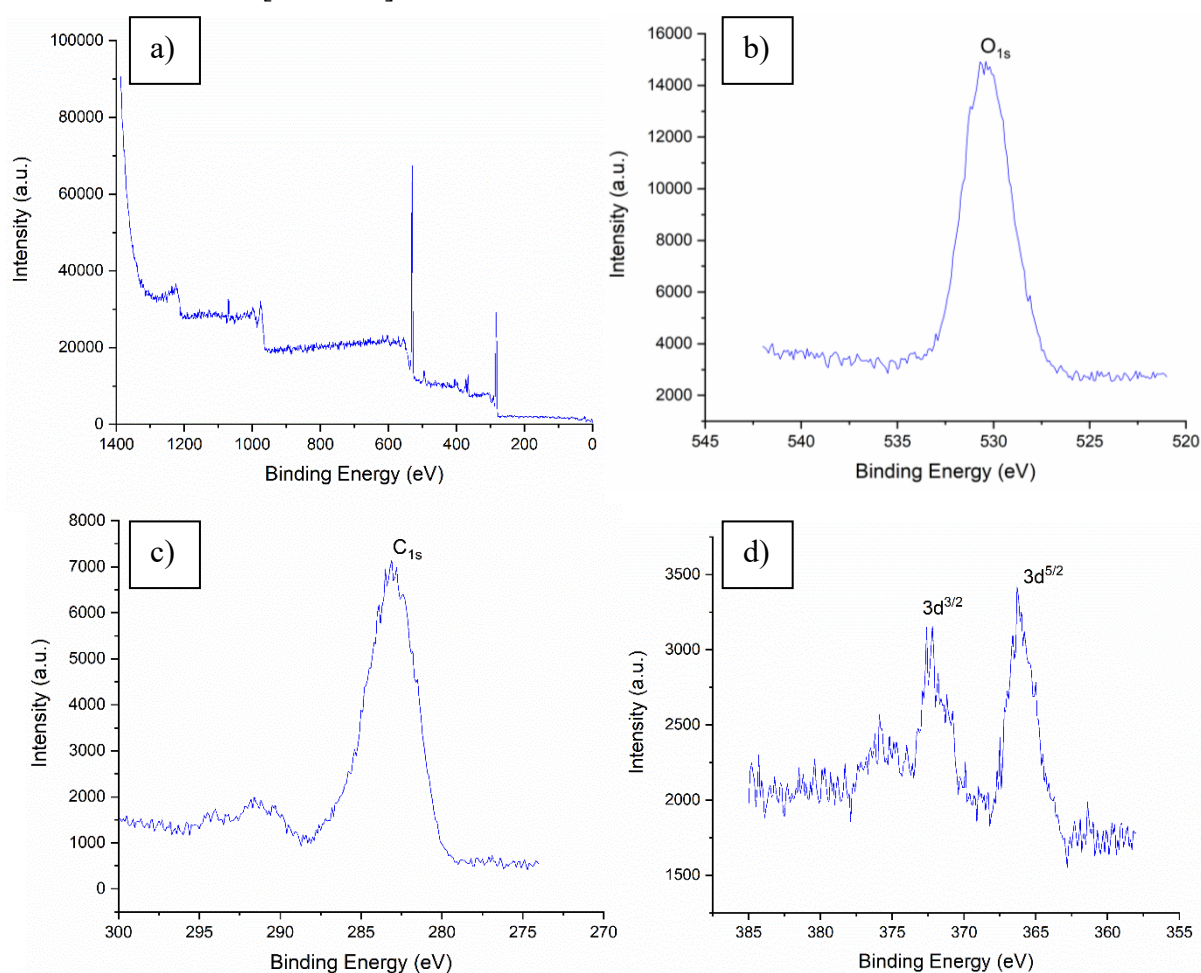
Figure 3. XPS results of PEG400/MTE-Ag NPs: a) XPS survey spectrum b) O_{1s}, c) C_{1s}, and d) Ag_{3d}.

Fig. 4a illustrates the TEM image of Ag NPs synthesized through plant-mediated ultrasound-assisted methods. The particles exhibit a spherical morphology with diameters smaller than 10 nm and are uniformly distributed in the colloidal solution. The distribution of the synthesized NPs is polydisperse, comprising particles of different sizes, without any agglomeration. Artificial intelligence (AI)-based Image J software (8-bit, 5-ramp mode) was utilized to verify the nanosize distribution of the nanostructures and demonstrate the absence of aggregation. (**Fig.4b**). This AI-based TEM analysis enabled us to determine the particle

nanosize distribution and identify any agglomerates present in the colloidal solution. The agglomerates were highlighted in green color particles within the red matrix. The results of this analysis provided additional support to our initial observation of a polydisperse distribution without any agglomeration.
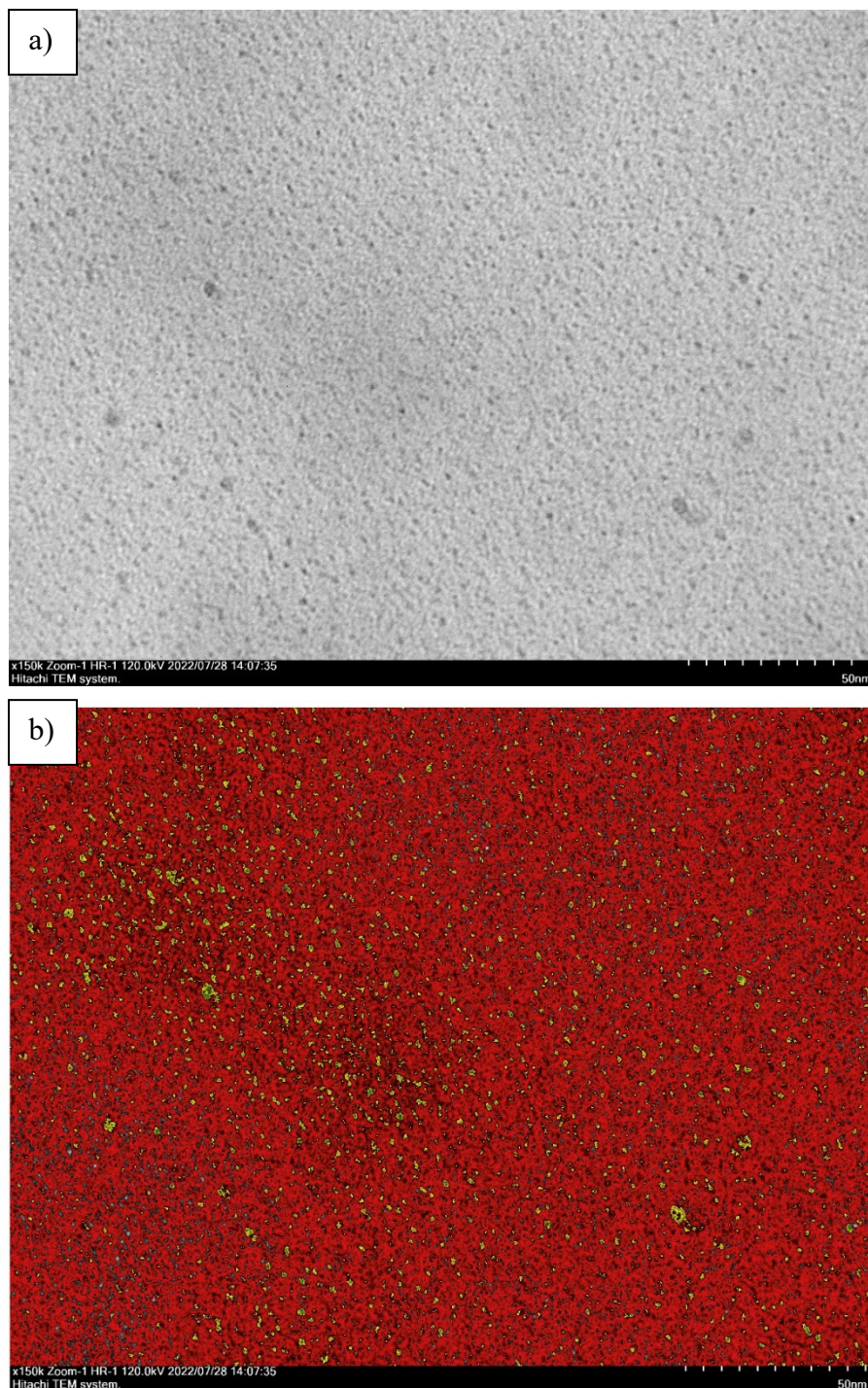
**Figure 4.** a) TEM and b) AI-based TEM image of the synthesized PEG400/MTE-Ag NPs

3.2. Characterization results of the coated SS316L

The distribution, shape, and agglomeration of PEG400/MTE-Ag NPs coated surfaces of SS316L were investigated using the SEM technique. SEM images uncoated and coated surface at x1000, x30000, and x50000, magnifications are shown in **Fig. 5a-d**, respectively. Micron-scaled cutting lines originating from the CNC process are clearly visible in the uncoated surface image (**Fig. 5a**). In the lower magnification surface view of coated surface (**Fig. 5b**), it is observed that the Ag NPs are distributed on the surface in a very smooth, homogeneous, and mono-layered manner. Additionally, the cutting line formed after the CNC cutting process is clearly visible on the surface. As seen in **Fig. 5c-d**, the NPs are spherical in shape. However, agglomeration occurred in some areas after the airbrush spraying process, which may have been caused by drying at room conditions. NPs with high surface area and thus surface energy are highly prone to agglomeration. In the literature, there are many studies in which metallic surfaces are modified with Ag NPs [19–21,30,31].
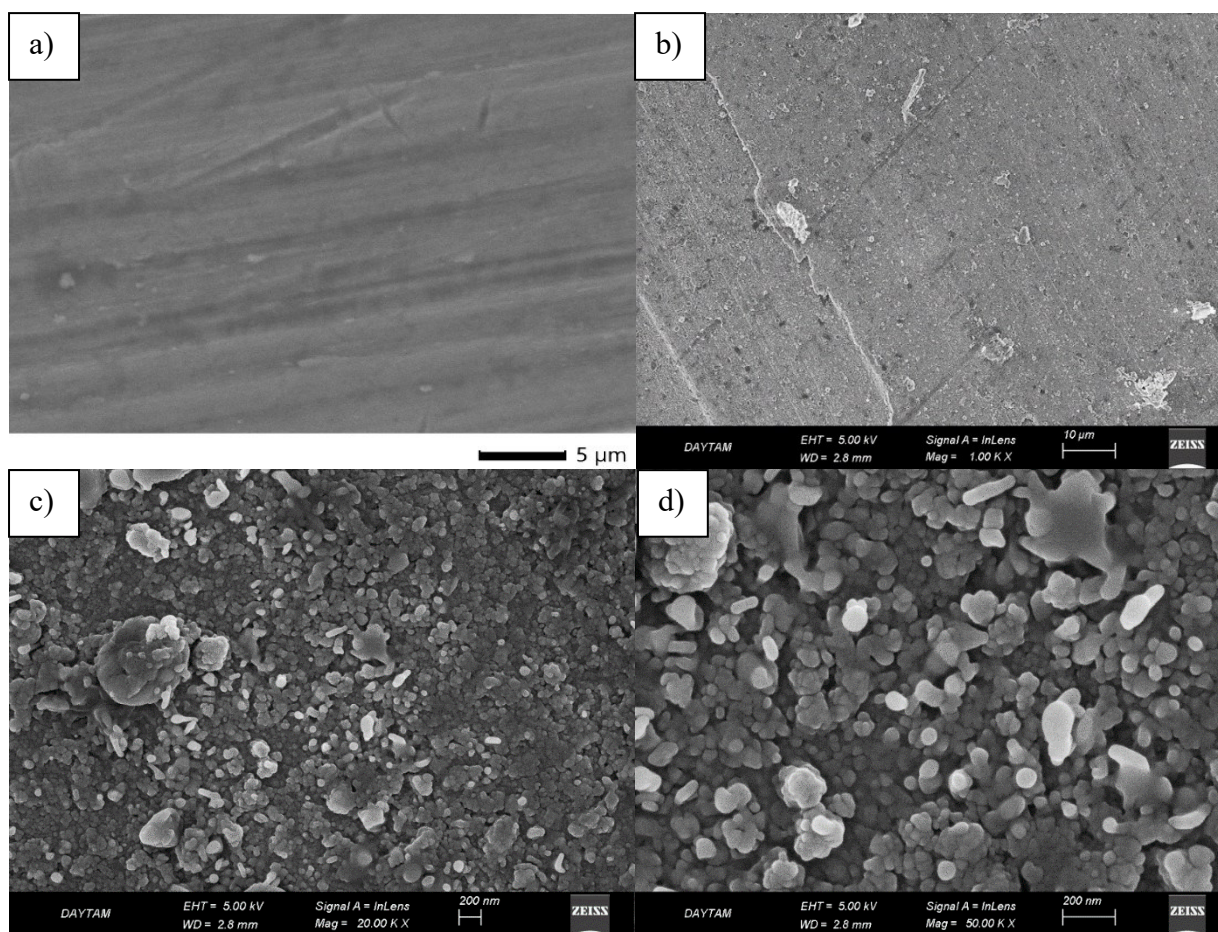
Figure 5. SEM images of the a) uncoated and PEG400/MTE-Ag NPs coated SS316L at different magnifications b) x1,000, c) x30,000, and d) x50,000

The cross-sectional image of the SS316L that has had its surface changed by Ag NPs was examined under an optical microscope. The analysis concentrated on the coating's thickness and dispersion across the surface as well as how it interacted with the substrate. In **Fig. 6**, a cross-sectional view of the coating surface is given. In the image, it is seen that the coating is distributed homogeneously and without creating any gaps on the surface. It is seen that the coating thicknesses vary regionally, and the coating distribution has a very homogeneous and void-free structure. There is no discontinuous region on the coating surface, and no cracks or delamination formations were observed. The average thickness value of the coating, as determined under the optical microscope, was found to be 2.476 µm.
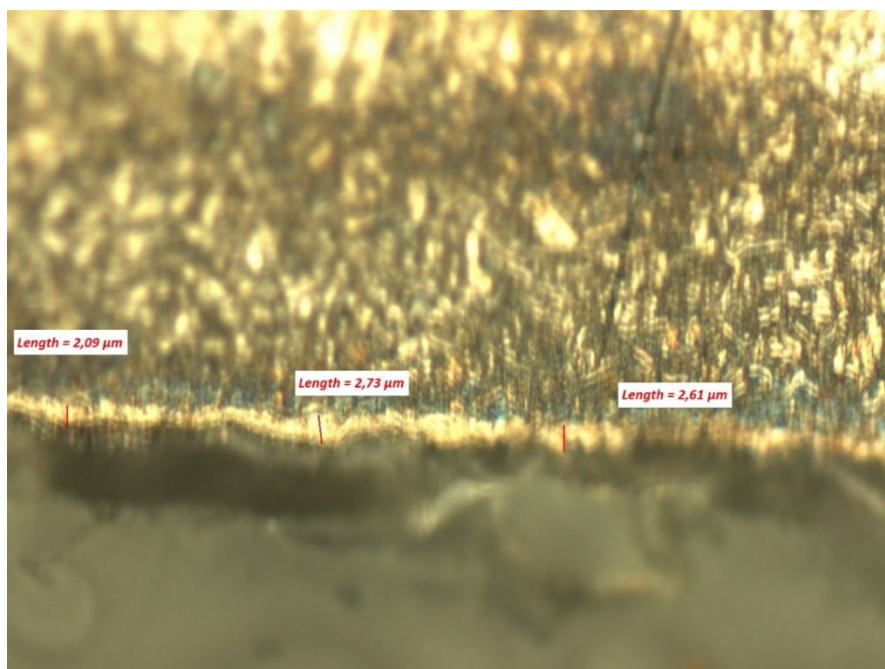

Figure 6. Cross-sectional image of the PEG400/MTE-Ag NPs coating

The surface roughness values of biomaterials are one of the important surface properties in the adaptation phase with the body. For this reason, surface roughness change was observed after coating. The **Table 2** presents the average surface roughness values unmodified and modified surface with PEG400/MTE-Ag NPs. After coating the surface with Ag NPs with the airbrush spray technique, a decrease of 11% was observed in the average surface roughness value. This is generally due to the fact that the micron-level depths formed on the surface after the CNC cutting process are filled with the nano-sized coating material. The desired surface roughness values on the surface of biometals are classified as medium (1-2 µm) and fine (0.5-1 µm) [32]. The average surface roughness values obtained after the coating was carried out in the study are compatible with the medium-level surface roughness values.

Table 2. Average surface roughness values

Uncoated Surface (Ra, µm)	Coated Surface (Ra, µm)	Changing (%)
1.328	1.182	-11

In order to examine the distribution, three-dimensional (3D) appearance, and thickness of the PEG400/MTE-Ag NPs coating on the SS316L, the coated surface was examined with a profilometer. The 3D view of the surface modified with Ag NPs by the airbrush spray coating technique is given in **Fig. 7**. It is seen that the Ag NPs are distributed quite homogeneously on the examined surface. The deep regions (black) observed on the surface represent the cutting lines in agreement with the SEM images (**Fig. 5c**). The coating thickness was determined as 3.97 µm. In the literature, Ag NPs-based coatings with a similar distribution are defined as a mono-layer homogeneous appearance [7,20]. The view of the final coating is consistent with the literature.
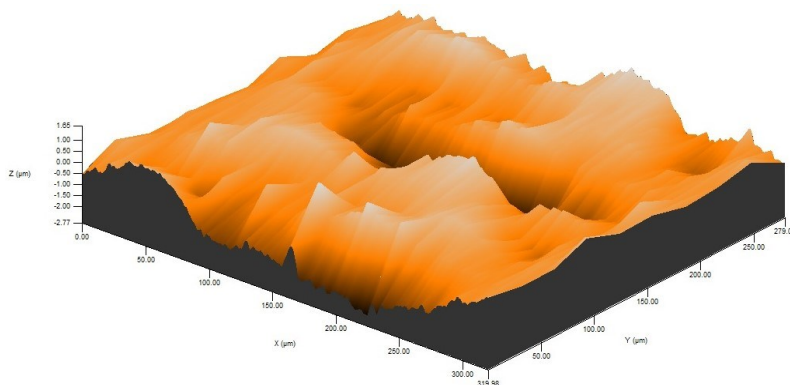
**Figure 7.** 3D surface profile of PEG400/MTE-Ag NPs coated SS316L

3.2.1. Antibacterial activity results

The antibacterial behavior of Ag-based structures has been known for many years. The bacterial resistance of Ag NPs-based nanobiocomposite coated SS316L were evaluated against two common post-implant reactions related pathogens in biomedical applications as known *E. coli* (gram-negative) and *S. aureus* (gram-positive), using the agar well diffusion method. In **Fig. 8a-d**, images of the after incubation were given uncoated SS316L in *E. coli* strain, coated sample in *E. coli* strain, uncoated SS316L in *S. aureus* strain, and coated sample in *S. aureus* strain, respectively. As expected, uncoated samples did not show any zone formation on either strain. The coated samples with PEG400/MTE-Ag NPs showed a zone of 22.4 mm in *E. coli* strain and 19.6 mm in *S. aureus* strain. Since the *E. coli* strain is a gram-negative pathogen, Ag^+ show more active behavior against *E.coli* strain [7,20,30]. The obtained ZOI values are consistent with the literature [20,30,33]. When the values are compared with the literature, it can be said that the final coating obtained in this study exhibits a more active behavior. It can be said that this is caused by the small size (<10 nm) and high surface area of the NPs [34,35].

3.2.2. Anticorrosive performance results

SS316L is prone to corrosion easily after contact with body fluids, so it is important to improve anticorrosive performance of surface. The open circuit potential (OCP) curve and potentiodynamic polarization (Tafel) curve in the Ringer solution of coated and uncoated SS316L samples are given in **Fig. 9a-b**. OCP curves give information about the stability of any material in the test medium. Material with high OCP value exhibits more stable behavior in that medium. In this study, during the electrochemical polarization tests conducted in Ringer's solution, the bare sample formed a curve at a value of -0.593 V, while the PEG400/MTE-Ag

NPs coated sample formed a curve at a value of -0.388 V, as shown in **Fig.9a**. This indicates that coated samples show more noble behavior in Ringer's solution. In the Tafel curves, it is stated that the sample with lower current density and higher potential exhibits better corrosion resistance [18,36]. Thus, **Fig. 9b** shows that the corrosion resistance of surface modified SS316L with Ag NP's has increased significantly. In the literature, corrosion resistance properties of surface-modified metallic surfaces with NPs by various methods have been investigated with different corrosion measurement techniques in various mediums such as NaCl [30,33], Ringer's solution [7,19], phosphate buffered solution [18]. In these studies, it was observed that the corrosion resistance changed at different times and mediums, and the corrosion resistance decreased especially in the NaCl environment. The corrosion resistance measurements performed in Ringer's solution in this study showed consistent results with similar studies in the literature.
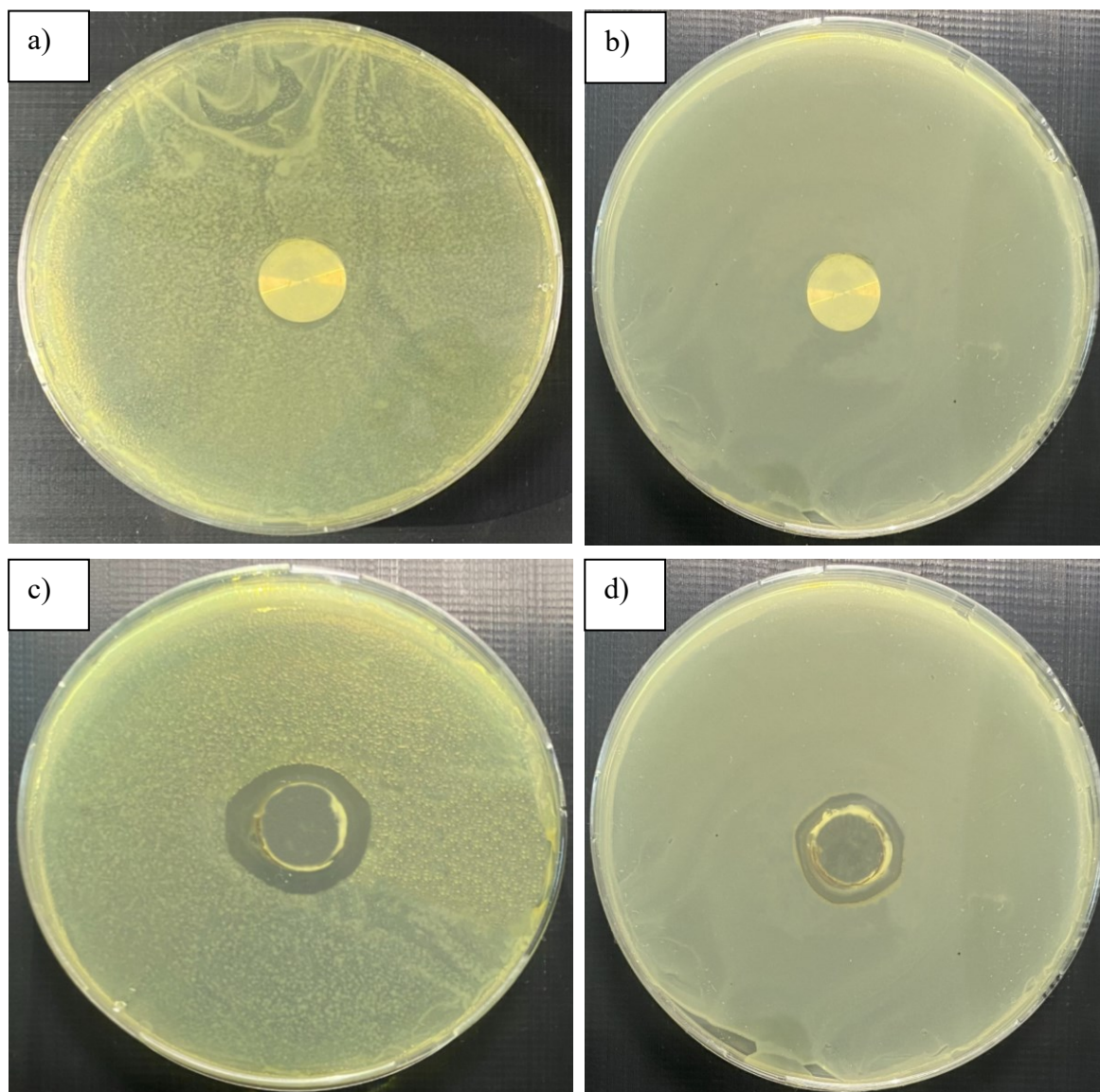
Figure 8. Antibacterial activity test results a) uncoated sample in *E. coli* strain b) uncoated sample in *S. aureus* strain, c) coated sample in *E. coli* strain, and d) coated sample in *S. aureus* strain.
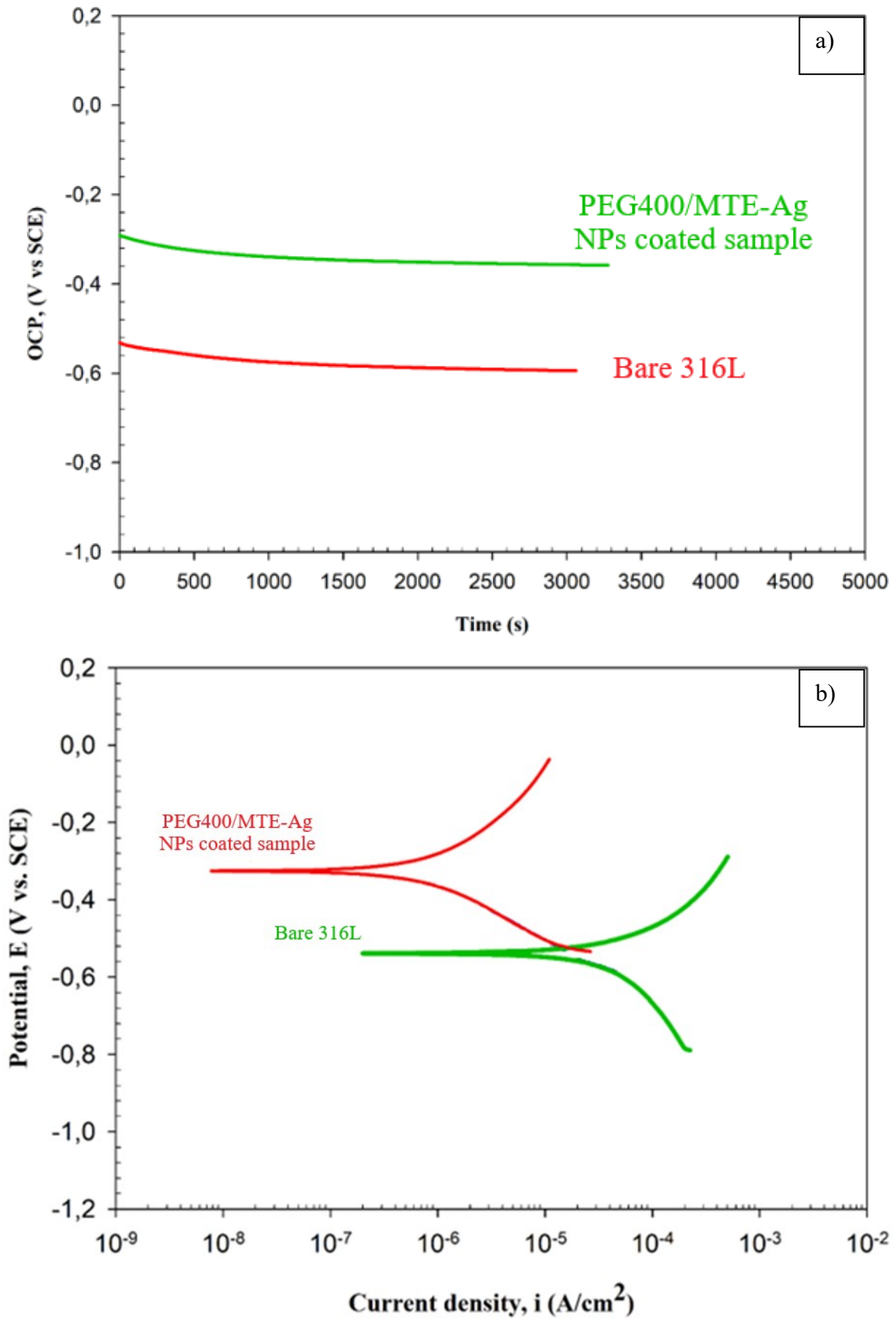
Figure 9. a) OCP and b) Tafel curves of uncoated and coated samples

4. Conclusion

In this study, the surface of the SS316L was modified with Ag NPs using plant extract-based synthesis. The plant-mediated synthesized Ag NPs and nanosized coating on the surface of SS316L were characterized by multifaceted investigations in order to enhance their applicability in the biomedical field. The main results of the study are summarized as follows:

- The Ag NPs in the bio-matrix displayed a spherical shape and homogeneous distribution, with a particle size of less than 10 nm.
- The PEG400/MTE-Ag NPs onto the surface of the superficially modified SS316L showed a fairly homogeneous distribution.
- A smooth and continuous interface was observed between the SS316L surface and the PEG400/MTE-Ag NPs layer without any micro-scale cracks. The coating thickness was consistent and remained in a monolayer without any significant changes.
- The average surface roughness value of the modified surface is medium in classification and this result indicates that the nanocoating has good biomedical application potential.
- Improvement of surface properties with Ag NPs coating SS316L effectively enhanced its electrochemical corrosion and antibacterial behavior.
- The development of multifunctional surfaces is both a technological and scientific challenge for medical applications. In this study, it has been shown that plant-mediated synthesized Ag NPs have an effective role in enhancing the properties of biometallic surfaces.
- This study could serve as a basis for researchers to develop new methods, strategies, and materials towards the design of cost-effective, environmentally sustainable, corrosion-resistant, and antibacterial nanomaterials.

Ethics in Publishing

There are no ethical issues regarding the publication of this study.

Author Contributions

All authors contributed equally to the writing of this manuscript.

Acknowledgements

References

[1] Hanawa, T. (2019). Overview of metals and applications. *Metals for Biomedical Devices*, 3–29. https://doi.org/10.1016/B978-0-08-102666-3.00001-8

[2] Ivanova, E. P., Bazaka, K., & Crawford, R. J. (2014). Metallic biomaterials: types and advanced applications. *New Functional Biomaterials for Medicine and Healthcare*, 121–147. https://doi.org/10.1533/9781782422662.121

[3] Mosas, K. K. A., Chandrasekar, A. R., Dasan, A., Pakseresht, A., & Galusek, D. (2022). Recent Advancements in Materials and Coatings for Biomedical Implants. *Gels 2022, Vol. 8, Page 323*, *8*(5), 323. https://doi.org/10.3390/GELS8050323

[4] Kumar, P., Duraipandy, N., Manikantan Syamala, K., & Rajendran, N. (2018). Antibacterial effects, biocompatibility and electrochemical behavior of zinc incorporated niobium oxide coating on 316L SS for biomedical applications. *Applied Surface Science*, *427*, 1166–1181. https://doi.org/10.1016/J.APSUSC.2017.08.221

[5] Kumar, M., Kumar, R., & Kumar, S. (2021). Coatings on orthopedic implants to overcome present problems and challenges: A focused review. *Materials Today: Proceedings*, *45*, 5269–5276. https://doi.org/10.1016/J.MATPR.2021.01.831

[6] Garcia-Lobato, M. A., Mtz-Enriquez, A. I., Garcia, C. R., Velazquez-Manzanares, M., Avalos-Belmontes, F., Ramos-Gonzalez, R., & Garcia-Cerda, L. A. (2019). Corrosion resistance and in vitro bioactivity of dense and porous titania coatings deposited on 316L SS by spraying method. *Applied Surface Science*, *484*, 975–980. https://doi.org/10.1016/J.APSUSC.2019.04.108

[7]   Karabulut, G., Beköz Üllen, N., Akyüz, E., & Karakuş, S. (2023). Surface modification of 316L stainless steel with multifunctional locust gum/polyethylene glycol-silver nanoparticles using different coating methods. *Progress in Organic Coatings*, *174*, 107291.

[8] Das, S., Sen, B., & Debnath, N. (2015). Recent trends in nanomaterials applications in environmental monitoring and remediation. *Environmental Science and Pollution Research 2015 22:23*, *22*(23), 18333–18344. https://doi.org/10.1007/S11356-015-5491-6

[9] Prema, P., Lakshmi Priya, S., & Rameshkumar, G. (2012). Bio-based and chemical mediated fabrication of silver nanoparticles and evaluation of their potential antimicrobial activity - A comparative view. *International Journal of Nanoparticles*, *5*(4), 338–357. https://doi.org/10.1504/IJNP.2012.049910

[10] Al-Sheddi, E. S., Farshori, N. N., Al-Oqail, M. M., Al-Massarani, S. M., Saquib, Q., Wahab, R., Musarrat, J., Al-Khedhairy, A. A., & Siddiqui, M. A. (2018). Anticancer potential of green synthesized silver nanoparticles using extract of nepeta deflersiana against human cervical cancer cells (HeLA). *Bioinorganic Chemistry and Applications*, *Nov*(1), 9390784. https://doi.org/10.1155/2018/9390784

[11] Rana, A., Yadav, K., & Jagadevan, S. (2020). A comprehensive review on green synthesis of nature-inspired metal nanoparticles: Mechanism, application and toxicity. *Journal of Cleaner Production*, *272*, 122880. https://doi.org/10.1016/j.jclepro.2020.122880

[12] Chavali, M. S., & Nikolova, M. P. (2019). Metal oxide nanoparticles and their applications in nanotechnology. *SN Applied Sciences 2019 1:6*, *1*(6), 1–30. https://doi.org/10.1007/S42452-019-0592-3

[13] Jamkhande, P. G., Ghule, N. W., Bamer, A. H., & Kalaskar, M. G. (2019). Metal nanoparticles synthesis: An overview on methods of preparation, advantages and disadvantages, and applications. *Journal of Drug Delivery Science and Technology*, *53*, 101174. https://doi.org/10.1016/j.jddst.2019.101174

[14] Ahmad, S., Munir, S., Zeb, N., Ullah, A., Khan, B., Ali, J., Bilal, M., Omer, M., Alamzeb, M., Salman, S. M., & Ali, S. (2019). Green nanotechnology: a review on green synthesis of silver nanoparticles — an ecofriendly approach. *International Journal of Nanomedicine*, *14*, 5087. https://doi.org/10.2147/IJN.S200254

[15] Karadirek, Ş., & Okkay, H. (2019). Ultrasound assisted green synthesis of silver nanoparticle attached activated carbon for levofloxacin adsorption. *Journal of the Taiwan Institute of Chemical Engineers*, *105*, 39–49. https://doi.org/10.1016/J.JTICE.2019.10.007

[16] Karakuş, S., Taşaltın, N., Taşaltın, C., & Üllen, N. B. (2021). Synthesis and Characterization of Konjac Gum/Polyethylene Glycol-Silver Nanoparticles and their Potential Application as a Colorimetric Sensor for Hydrogen Peroxide. *Journal of Inorganic and Organometallic Polymers and Materials*, *31*(9), 3726–3739. https://doi.org/10.1007/S10904-021-01984-5

[17] Tan, E., Kahyaoğlu, İ. M., & Karakuş, S. (2021). A sensitive and smartphone colorimetric assay for the detection of hydrogen peroxide based on antibacterial and antifungal matcha extract silver nanoparticles enriched with polyphenol. *Polymer Bulletin*, 1–27. https://doi.org/10.1007/S00289-021-03857

[18] Zhang, S., Liang, X., Gadd, G. M., & Zhao, Q. (2021). A sol–gel based silver nanoparticle/polytetrafluorethylene (AgNP/PTFE) coating with enhanced antibacterial and anti-corrosive properties. *Applied Surface Science*, *535*, 147675. https://doi.org/10.1016/J.APSUSC.2020.147675

[19] Abdulsada, F. W., & Hammood, A. S. (2021b). Characterization of corrosion and antibacterial resistance of hydroxyapatite/silver nano particles powder on 2507 duplex stainless steel. *Materials Today: Proceedings*, *42*, 2301–2307. https://doi.org/10.1016/J.MATPR.2020.12.319

[20] Alias, R., Mahmoodian, R., & Abd Shukor, M. H. (2019). Development and characterization of a multilayer silver/silver-tantalum oxide thin film coating on stainless steel for biomedical applications. *International Journal of Adhesion and Adhesives*, *92*, 89–98. https://doi.org/10.1016/J.IJADHADH.2019.04.010

[21] Aminatun, Furqon, I. A., Hikmawati, D., & Abdullah, C. A. C. (2021). Antibacterial Properties of Silver Nanoparticle (AgNPs) on Stainless Steel 316L. *Nanomedicine Research Journal*, *6*(2), 117–127. https://doi.org/10.22034/NMRJ.2021.02.004

[22] Abbas, A., & Amin, H. M. A. (2022). Silver nanoparticles modified electrodes for electroanalysis: An updated review and a perspective. *Microchemical Journal*, *175*, 107166. https://doi.org/10.1016/J.MICROC.2021.107166

[23] Soe, H. M., Abd Manaf, A., Matsuda, A., & Jaafar, M. (2021). Performance of a silver nanoparticles-based polydimethylsiloxane composite strain sensor produced using different fabrication methods. *Sensors and Actuators A: Physical*, *329*, 112793. https://doi.org/10.1016/J.SNA.2021.112793

[24] Santhosh, A., Theertha, V., Prakash, P., & Smitha Chandran, S. (2021). From waste to a value added product: Green synthesis of silver nanoparticles from onion peels together with its diverse applications. *Materials Today: Proceedings*, *46*, 4460–4463. https://doi.org/10.1016/J.MATPR.2020.09.680

[25] Gulbagca, F., Ozdemir, S., Gulcan, M., & Sen, F. (2019). Synthesis and characterization of Rosa canina-mediated biogenic silver nanoparticles for anti-oxidant, antibacterial, antifungal, and DNA cleavage activities. *Heliyon*, *5*(12), e02980. https://doi.org/10.1016/J.HELIYON.2019.E02980

[26] Gomathi, M., Rajkumar, P. V., Prakasam, A., & Ravichandran, K. (2017). Green synthesis of silver nanoparticles using Datura stramonium leaf extract and assessment of their antibacterial activity. *Resource-Efficient Technologies*, *3*(3), 280–284. https://doi.org/10.1016/J.REFFIT.2016.12.005

[27] Mallikarjuna, K., John Sushma, N., Narasimha, G., Manoj, L., & Deva Prasad Raju, B. (2014). Phytochemical fabrication and characterization of silver nanoparticles by using Pepper leaf broth. *Arabian Journal of Chemistry*, *7*(6), 1099–1103. https://doi.org/10.1016/J.ARABJC.2012.04.001

[28] LewisOscar, F., Nithya, C., Vismaya, S., Arunkumar, M., Pugazhendhi, A., Nguyen-Tri, P., Alharbi, S. A., Alharbi, N. S., & Thajuddin, N. (2021). In vitro analysis of green fabricated silver nanoparticles (AgNPs) against Pseudomonas aeruginosa PA14 biofilm formation, their application on urinary catheter. *Progress in Organic Coatings*, *151*, 106058. https://doi.org/10.1016/J.PORGCOAT.2020.106058

[29] Aygün, A., Özdemir, S., Gülcan, M., Cellat, K., & Şen, F. (2020). Synthesis and characterization of Reishi mushroom-mediated green synthesis of silver nanoparticles for the biochemical applications. *Journal of Pharmaceutical and Biomedical Analysis*, *178*, 112970. https://doi.org/10.1016/J.JPBA.2019.112970

[30] Jeeva Jothi, K., Balachandran, S., & Palanivelu, K. (2022). Synergistic combination of Phyllanthus niruri / silver nanoparticles for anticorrosive application. *Materials Chemistry and Physics*, *279*, 125794. https://doi.org/10.1016/J.MATCHEMPHYS.2022.125794

[31] Soloviev, M., & Gedanken, A. (2011). Coating a stainless steel plate with silver nanoparticles by the sonochemical method. *Ultrasonics Sonochemistry*, *18*(1), 356–362. https://doi.org/10.1016/J.ULTSONCH.2010.06.015

[32] Albrektsson, T., & Wennerberg, A. (2004). Oral implant surfaces: Part 1--review focusing on topographic and chemical properties of different surfaces and in vivo responses to them. *The International Journal of Prosthodontics*, *17*(5), 536–543.

[33] Qian, H., Li, M., Li, Z., Lou, Y., Huang, L., Zhang, D., Xu, D., Du, C., Lu, L., & Gao, J. (2017). Mussel-inspired superhydrophobic surfaces with enhanced corrosion resistance and dual-action antibacterial properties. *Materials Science and Engineering: C*, *80*, 566–577. https://doi.org/10.1016/J.MSEC.2017.07.002

[34] Panáček, A., Kvítek, L., Prucek, R., Kolář, M., Večeřová, R., Pizúrová, N., Sharma, V. K., Nevěčná, T., & Zbořil, R. (2006). Silver colloid nanoparticles: Synthesis, characterization, and their antibacterial activity. *Journal of Physical Chemistry B*, *110*(33), 16248–16253. https://doi.org/10.1021/JP063826H/SUPPL_FILE/JP063826HSI20060619_085949.PDF

[35] Pal, S., Tak, Y. K., & Song, J. M. (2007). Does the antibacterial activity of silver nanoparticles depend on the shape of the nanoparticle? A study of the Gram-negative bacterium Escherichia coli. *Applied and Environmental Microbiology*, *73*(6), 1712–1720. https://doi.org/10.1128/AEM.02218-06